J. Fluid Mech. (2005), *vol.* 534, *pp.* 97–114.
doi:10.1017/S0022112005004623 Printed in the United Kingdom

An analytic form for the pair distribution function and rheology of a dilute suspension of rough spheres in plane strain flow

By HELEN J. WILSON†

Department of Applied Mathematics, University of Leeds, Leeds LS2 9JT, UK

(Received 11 February 2003 and in revised form 2 February 2005)

The effect of particle–particle contact on the stress of a suspension of small spheres in plane strain flow is investigated. We provide an analytic form for the particle pair distribution function in the case of no Brownian motion, and calculate the viscosity and normal stress difference based on this. We show that the viscosity is reduced by contact, and a normal stress difference induced, both at order c^2 for small particle volume concentration c. In addition, we investigate the effect of a small amount of diffusion on the structure of the distribution function, giving a self-consistent form for the density in the $O(aPe^{-1})$ boundary layer and demonstrating that diffusion reduces the magnitude of the contact effect but does not qualitatively alter it.

1. Introduction

The study of suspensions of small particles has been of interest to scientists for many years, and is still an active area of research. Brady & Morris (1997) and Bergenholtz, Brady & Vicic (2002) have identified the need to focus attention on the effect of strong flows: that is, flows in which the non-dimensional flow rate is large relative to Brownian effects.

A major factor in the current understanding of colloid rheology has been the theoretical study of suspensions which are sufficiently dilute that only pairwise interactions need be considered (Batchelor & Green 1972*a*, *b*; Batchelor 1977). Later work by Russel (1980) and Bergenholtz *et al.* (2002) has shown that these pair-interaction calculations, which give results correct up to second order in the volume fraction c, can shed light on the behaviour of much more concentrated suspensions.

In this paper, we will consider the strong flow, non-Brownian limit of flow of a dilute suspension of rough particles. Using a simple effective hard-sphere model of rough particle contact, we show that for a plane straining flow the particle pair distribution can be calculated analytically in terms of standard mobility functions (see, for example Kim & Karrila 1991). This provides a checkpoint for finite-Péclet-number studies of straining flows such as Brady & Morris (1997), which cannot be provided for shear flows (except in two dimensions as in Wilson & Davis 2002) because of regions of particle trajectory space in which particles remain bound forever. We use the particle pair distribution function to calculate the deviatoric part of the effective stress of a dilute suspension of rough spheres in plane strain, and show that the $O(c^2)$ coefficient in the expansion for the viscosity is lowered by the presence of particle roughness,

† Present address: Department of Mathematics, University College London, Gower Street, London WC1E 6BT, UK; helen.wilson@ucl.ac.uk.

and the second normal stress difference caused at second order in c is negative (using the conventions of Brady & Morris 1997): that is, the average of the diagonal stresses along the compressional and extensional axes is less than the diagonal stress along the neutral axis. We also illustrate how addition of a small amount of Brownian motion would affect these quantities, and compare these results with finite-Péclet-number results from Brady & Morris (1997).

In § 2, we pose the problem rigorously, and set up our geometrical parameters. In §§ 3, 4 and 5 we outline the details of the calculation for the pair distribution function, contact force and stress, respectively. The results are presented in § 6. Concluding remarks, including a discussion of the case of large finite Péclet number, are given in § 7.

2. Formulation of the problem

We consider a Newtonian fluid of viscosity μ, containing neutrally buoyant suspended solid spherical particles of radius a at volume fraction c. The only forces acting on the particles are hydrodynamic forces and short-range contact forces. The derivation of the particle pair distribution and stresses will essentially follow the model of Zinchenko (1984) and Wilson & Davis (2000), but the geometrical change, to a plane straining flow, necessitates some detailed explanation.

2.1. *Flow field*

The far-field velocity is imposed as the linear function $\boldsymbol{U}^{\infty} = \boldsymbol{E} \cdot \boldsymbol{x}$, where

$$\boldsymbol{E} = \begin{pmatrix} \dot{\epsilon} & 0 & 0 \\ 0 & -\dot{\epsilon} & 0 \\ 0 & 0 & 0 \end{pmatrix} \tag{2.1}$$

represents a planar strain flow far from any particles. The suspension takes on this velocity only in an average sense, as the presence of rigid particles and the interactions between them affect the local flow.

The bulk stress tensor in the suspension (where the solvent has Newtonian viscosity μ) is given by

$$\Sigma_{ij} = -p\delta_{ij} + 2\mu E_{ij} - p^{(p)}\delta_{ij} + \Sigma_{ij}^{(p)}, \tag{2.2}$$

where the total particle stress $-p^{(p)}\delta_{ij} + \Sigma_{ij}^{(p)}$ (deriving from the rigidity of a particle in its interaction with the surrounding suspension, and from inter-particle forces) is summed over all particles, and $\Sigma_{ij}^{(p)}$ is deviatoric. The isotropic contribution $p^{(p)}$ is the perturbation to the pressure in the fluid caused by the presence of the particles (Brady 1993). Although resistance functions do exist for this quantity (P and Q of Jeffrey, Morris & Brady 1993), methods for calculating them are not easily available and we will not calculate $p^{(p)}$ here. For a suspension in which the solid volume fraction and shear rate are both constant, the addition of a constant particle pressure will not affect the flow, as for an incompressible fluid, the pure hydrodynamic pressure, p, is arbitrary, and has no direct effect on flow; however, in the presence of gradients of concentration or shear rate, these terms could be important.

By exploiting the symmetry of the flow, with no further information we can show that the symmetric, deviatoric particle stress must have the form

$$\boldsymbol{\Sigma}^{(p)} = \begin{pmatrix} 2\mu^*\dot{\epsilon} + \frac{1}{3}N_2 & 0 & 0 \\ 0 & -2\mu^*\dot{\epsilon} + \frac{1}{3}N_2 & 0 \\ 0 & 0 & -\frac{2}{3}N_2 \end{pmatrix} \tag{2.3}$$

where the second normal stress difference N_2 is defined according to the convention used by Brady & Morris (1997), when conversion is made from their axes on which $E_{ij} = \dot{\epsilon}(\delta_{i1}\delta_{j2} + \delta_{i2}\delta_{j1})$. We will show analytic results for μ^* and N_2 to order c^2 in the particle concentration.

2.2. *Contact model*

We will consider the simplest possible model of inter-particle contact. In this model, when two particles come into contact, they behave according to hard-sphere repulsion. This is included within the roll-slip models of Davis (1992) and Ekiel-Jeżewska *et al.* (1999). At an inter-particle surface-surface separation $h_c = a\zeta$, with $\zeta \ll 1$, their approach is halted by small surface asperities. They remain in contact (with the minimum gap between their nominal surfaces equal to h_c) for as long as the net hydrodynamic forces acting on them are compressive. Once the hydrodynamic forces act to separate the spheres, the contact breaks and there is no contact force; the particles separate unhindered except by hydrodynamic forces. While the particles are in contact, the contact force is parallel to the line of centres of the two spheres, and on each sphere, is equal and opposite to the normal hydrodynamic force on that sphere. This model has just one dimensionless parameter, ζ, with suggested physical values of $10^{-3} < \zeta < 10^{-2}$ (from Smart & Leighton 1989) or $3 \times 10^{-5} < \zeta < 3 \times 10^{-3}$ (from Ekiel-Jeżewska *et al.* 1999). In generating numerical values for macroscopic physical quantities such as viscosity, we will consider the range $0 \leqslant \zeta \leqslant 10^{-2}$.

2.3. *Calculation of stress*

The detailed description of the general method of calculating macroscopic fluid stress of a dilute suspension in a linear flow field to $O(c^2)$ (with smooth particles) can be found in Batchelor (1967, pp. 246–253), and the changes caused by contact interactions in Wilson & Davis (2000). Here we present only a summary of the method, introducing the changes required for the geometry of plane strain. We expand the extra (particle) stress in powers of the small volume concentration, c, while averaging over the volume of the suspension.

The leading-order term (which is $O(c)$) is derived from consideration of the extra dissipation caused by an isolated sphere in the far-field flow $\boldsymbol{U}^\infty$, and was calculated by Einstein (1906, 1911). The $O(c^2)$ term (first calculated by Batchelor & Green 1972*a*, *b*) is caused by binary interactions between pairs of particles. The total extra stress may be expressed (as in Wilson & Davis 2000, equations (2.5) and (2.6)) as

$$\begin{aligned}\boldsymbol{\Sigma}^{(p)} = {} & 5c\mu\boldsymbol{E} + 5c^2\mu\boldsymbol{E} + \frac{9c^2}{64\pi^2a^5}\int_{contact} F_c s(1-A(s))\left[\boldsymbol{nn} - \tfrac{1}{3}\boldsymbol{I}\right] p(\boldsymbol{r})\,\mathrm{d}\boldsymbol{r} \\ & + \frac{15c^2\mu}{4\pi a^3}\int_{r\geqslant 2a} [K(s)\boldsymbol{E} + [(\boldsymbol{E}\cdot\boldsymbol{n})\boldsymbol{n} + \boldsymbol{n}(\boldsymbol{E}\cdot\boldsymbol{n})]L(s) \\ & + (\boldsymbol{n}\cdot\boldsymbol{E}\cdot\boldsymbol{n})\left[\boldsymbol{nn}M(s) - \left(\tfrac{2}{3}L(s) + \tfrac{1}{3}M(s)\right)\boldsymbol{I}\right]\Big]\, p(\boldsymbol{r})\,\mathrm{d}\boldsymbol{r} + O(c^3), \end{aligned} \tag{2.4}$$

in which $\boldsymbol{n} = \boldsymbol{r}/r$, $s = r/a$, and $p(\boldsymbol{r})$ is the pair distribution function: the scaled probability of finding a particle at $\boldsymbol{x}_0 + \boldsymbol{r}$ given that a particle is at $\boldsymbol{x}_0$. The scalar quantity F_c is such that the contact force exerted on the particle at $\boldsymbol{x}_0$ by the other is $F_c\boldsymbol{n}$, acting along the line of centres of the particles as discussed above. Two terms have been altered from the most general form given in Wilson & Davis (2000): Batchelor's renormalization term is omitted from the integral since it does not contribute *provided the angle integrals are carried out first*; and the stress contributed directly by the contact force has been specified to forces with no tangential component. The hydrodynamic

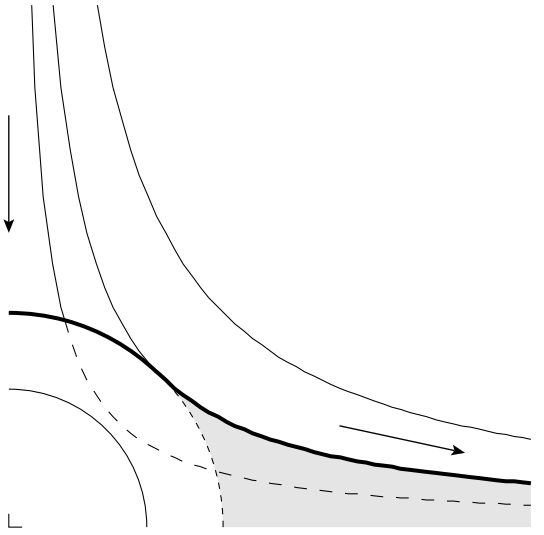

FIGURE 1. Schematic quarter cross-section of the trajectories of the centre of particle 2 relative to the centre of particle 1 in planar straining flow. The inner circle has radius $2a$; the outer, radius $a(2+\zeta)$, where the dimensionless roughness height ζ is inflated for illustrative purposes. The long dashed line indicates a trajectory which would have been followed in the absence of inter-particle forces; with contact forces, the trajectory is deflected onto the thick line.

functions A, K, L and M, along with B and J, have been thoroughly investigated in previous work (see, for example, Kim & Karrila 1991).

Apart from the contact force, the only unknown quantity in (2.4) is the pair distribution function $p(\boldsymbol{r})$. This is defined as the probability of finding a particle centred at $\boldsymbol{x}_0+\boldsymbol{r}$ given that there is a particle centred at $\boldsymbol{x}_0$ (normalized so that $p(\boldsymbol{r})\to 1$ as $r\to\infty$). In the non-Brownian limit, this function is governed by the Liouville equation (Batchelor & Green 1972*a*):

$$\nabla\cdot[\,p(\boldsymbol{r})\boldsymbol{V}(\boldsymbol{r})]=0, \tag{2.5}$$

where $\boldsymbol{V}$ is the velocity of the centre of particle 2 relative to the centre of particle 1 when their instantaneous displacement is $\boldsymbol{r}$. We use a trajectory-style analysis to calculate the pair-distribution function analytically. This ability is the major reason why this full calculation is possible: if Brownian motion is not neglected then approximations must be made (as in, for example, Brady & Morris 1997, in which only the compressive quadrant of the flow is considered).

2.4. *Geometrical analysis*

We consider the interaction between two spheres, as specified above, labelled 1 and 2. We place particle 1 instantaneously at the origin of the linear flow field $\boldsymbol{U}^\infty$, and particle 2 at $\boldsymbol{r}$. The inter-particle separation is r, with dimensionless value $s=r/a$. The particles make contact at $s=s_c\equiv 2+\zeta$ (where ζ is the dimensionless roughness height). Throughout this paper, we denote the value of a mobility function at this separation as $X_c=X(s=s_c)$.

Part of a cross-section of the trajectories swept out by the centre of particle 2 (relative to the centre of particle 1) is shown schematically in figure 1. Particles come in in the y-direction and leave in the x-direction. Note that, when the trajectory for smooth spheres reaches the boundary $s=2+\zeta$, it is deflected. Outside the limiting

trajectory along which the two particles just come into contact, the behaviour of the system is exactly as it would be for perfectly smooth spheres.

The system, including the effect of particle–particle contacts, is symmetric about the planes $x=0$, $y=0$ and $z=0$, so we consider only the region $x>0$, $y>0$, $z>0$, and multiply the stress contribution from each region by a factor of 8 to regain the total stress. The pair distribution function has a fore–aft asymmetry, and this octant contains both fore and aft regions (see figure 1).

At this point, we introduce spherical polar coordinates (s, θ, ϕ) for the position of the centre of particle 2 relative to the centre of particle 1, defined as

$$x = as\sin\theta\cos\phi; \quad y = as\sin\theta\sin\phi; \quad z = as\cos\theta. \tag{2.6}$$

Since the particles can never be closer than $s=s_c$, the space within which we need to calculate $p(\boldsymbol{r})$ is given by $s_c \leqslant s < \infty$, $0 \leqslant \theta \leqslant \pi/2$, $0 \leqslant \phi \leqslant \pi/2$.

When the particles are well separated ($s > s_c$), their relative velocity is given by the standard form:

$$\boldsymbol{V} = as[(1-B(s))\boldsymbol{E}\cdot\boldsymbol{n} + (B(s)-A(s))(\boldsymbol{n}\cdot\boldsymbol{E}\cdot\boldsymbol{n})\boldsymbol{n}]. \tag{2.7}$$

Using (2.1), this leads to particle trajectories given by

$$xy = a^2\xi_1\Phi^2(s); \quad z = a\xi_2\Phi(s) \tag{2.8}$$

in which

$$\Phi(s) = \exp\left[\int_s^\infty \frac{(A(s')-B(s'))}{1-A(s')}\frac{\mathrm{d}s'}{s'}\right] \tag{2.9}$$

and the parameters ξ_1 and ξ_2, which may take any values, are constant on a given trajectory.

Particles in contact move under the influence of a contact force which simply maintains their separation at s_c without affecting their tangential motion, so the relative velocity in contact is given by

$$\boldsymbol{V}^c = as_c\dot{\epsilon}(1-B_c)\sin\theta[\cos\theta\cos 2\phi\boldsymbol{e}_\theta - \sin 2\phi\boldsymbol{e}_\phi]. \tag{2.10}$$

This velocity matches the free velocity (2.7) where $s=s_c$ and $\phi=\pi/4$ since $\boldsymbol{n}\cdot\boldsymbol{E}\cdot\boldsymbol{n}=0$ there.

Referring back to figure 1, we can see that there are two types of trajectories (particle paths): those which do not intersect the contact surface $s=s_c$, and those which do. Particles on the former trajectories move unaffected by contact (with velocity $\boldsymbol{V}$ of (2.7)) throughout their motion. Those on the latter trajectories move unaffected by contact until they reach $s=s_c$, when their velocity changes discontinuously to $\boldsymbol{V}^c$ of (2.10) and they move within the contact surface. This causes a buildup of particle density on the contact surface. Such particles remain on the contact surface as long as the contact force required to hold them there is compressive; that is, as long as $\boldsymbol{n}\cdot\boldsymbol{E}\cdot\boldsymbol{n}<0$. At the point where $\boldsymbol{n}\cdot\boldsymbol{E}\cdot\boldsymbol{n}=0$, the contact force ceases and the particles once more have relative velocity given by (2.7). However, all particles which have experienced contact leave the contact surface on the same set of trajectories, and the density which has built up on the contact surface is swept out on a 'sheet' of high particle probability.

The shaded region of figure 1 represents positions where particle 2 cannot be found (once steady state is attained). To arrive at these positions, the particle would have to pass along a portion of trajectory with $s<s_c$, which is forbidden by the contact.

This forbidden 'wake' region is divided from the region of ordinary trajectories which have not undergone contact by the 'sheet' region introduced above.

In summary, we can divide our space into regions of different types:

(i) the bulk of space, for which the particle trajectories are unaffected by microscopic particle roughness: this includes trajectories which do not experience contact and the incoming part of all other trajectories before they reach contact separation;

(ii) the empty wake (shaded region) which exists because the particle–particle contacts support compressive, but not tensile, forces;

(iii) that part of the surface $s = s_c$ on which two particles are in contact; and

(iv) the 'sheet' in space separating the bulk region (i) from the empty wake (ii).

If we introduce a new mobility function

$$F(s) = s_c \Phi(s)/(s\Phi_c), \tag{2.11}$$

then these regions are defined geometrically as follows:

$$\text{Wake:}\ \ s_c \leqslant s < \infty, \quad 0 \leqslant \cos\theta \leqslant F(s), \quad 0 \leqslant \sin 2\phi \leqslant \frac{F^2(s) - \cos^2\theta}{\sin^2\theta}, \tag{2.12}$$

$$\text{Bulk:}\ \ \{s_c < s < \infty\} - \text{Wake}, \tag{2.13}$$

$$\text{Contact:}\ \ s = s_c, \quad 0 \leqslant \theta \leqslant \pi, \quad \pi/4 \leqslant \phi \leqslant \pi/2, \tag{2.14}$$

$$\text{Sheet:}\ \ s_c \leqslant s < \infty, \quad 0 \leqslant \cos\theta \leqslant F(s), \quad \sin 2\phi = \frac{F^2(s) - \cos^2\theta}{\sin^2\theta}. \tag{2.15}$$

In the extensional region of the flow, a trajectory which passed through the position $(s_c, \theta_0, \pi/4)$ and forms part of the sheet region, will later pass through a position (s, θ, ϕ_s) and we can reinterpret the mobility function $F(s)$ as the ratio $\cos\theta/\cos\theta_0$ (§ 3.4).

3. Pair distribution function

In the non-Brownian limit, we can solve the Liouville equation (2.5) in each of our regions to find the particle pair distribution function $p(\boldsymbol{r})$.

3.1. *Bulk region*

In the bulk (region (i)), the particle velocity, and hence the pair distribution function, is unaffected by particle contacts. It was shown by Batchelor & Green (1972*a*) that, for any material point which has come from infinity during the history of the flow, and has not been involved in a contact, the probability density at that point may be expressed as

$$p(\boldsymbol{r}) = q(s) = \frac{\Phi^{-3}(s)}{(1 - A(s))}, \tag{3.1}$$

where $\Phi(s)$ is as defined in (2.9), and $q(s) \to 1$ as $s \to \infty$.

3.2. *Wake region*

In the wake (region (ii)), there can be no particles so the pair distribution function is $p(\boldsymbol{r}) = 0$ and this region does not contribute to the stress.

3.3. *Contact region*

On the contact surface (region (iii)), we introduce a contact pair distribution function $P^c\delta(s - s_c) = ap(\boldsymbol{r})$. For values of s just larger than s_c, we have $V_r = as(1 - A)(\boldsymbol{n} \cdot \boldsymbol{E} \cdot \boldsymbol{n})$, but at $s = s_c$ we have no radial velocity. This means that the Liouville equation can

be rewritten as

$$0 = \nabla \cdot [P^c \boldsymbol{V}^c] + p(s_c^+) V_r = \nabla_s \cdot [P^c \boldsymbol{V}^c] + a s_c \Phi_c^{-3} \boldsymbol{n} \cdot \boldsymbol{E} \cdot \boldsymbol{n}, \tag{3.2}$$

where $\nabla_s \cdot \boldsymbol{u}$ is the surface divergence of $\boldsymbol{u}$. Using the velocity (2.10), this equation may be solved, discarding unphysical solutions with singularities at $\theta = \pi/2$, to produce

$$P^c = \frac{a s_c}{3(1 - B_c)\Phi_c^3}. \tag{3.3}$$

3.4. *Sheet region*

The sheet region (region (iv)) may be parameterized in terms of s and θ_0 (2.15):

$$\cos\theta = F(s)\cos\theta_0, \quad \sin 2\phi = F^2(s)\sin^2\theta_0 / \sin^2\theta, \tag{3.4}$$

where all points with the same value of θ_0 lie on a trajectory which passes through $(s_c, \theta_0, \pi/4)$. Within this region, the particles are not in contact, so their relative velocity is given by (2.7) and the probability distribution is governed by the Liouville equation (2.5).

Let us introduce the sheet probability density $ap(\boldsymbol{r}) = P^s \delta(\sin 2\phi - \sin 2\phi_s)$, where ϕ_s is the value of ϕ which lies in the sheet for a given pair (s, θ_0).

The value of this probability density at the point where the sheet leaves the contact surface is determined by the condition that p must be continuous at the point $(s_c, \theta_0, \pi/4)$. The velocity is continuous at this point so the only difficulty is the change of variables in the delta-function inherent in the probability field.

Within the sheet region, we use the standard form for a change of variables in a δ-function:

$$\delta(u - \overline{u}) = \frac{1}{|f'(s)|}\delta(s - \overline{s})$$

in which $u = f(s)$ and $\overline{u} = f(\overline{s})$. In this case, we use $u = \sin 2\phi$ to have, from (3.4),

$$f(s) = \frac{F^2(s)\sin^2\theta_0}{\sin^2\theta} = \tan^2\theta_0 \left[\frac{1}{1 - F^2(s)\cos^2\theta_0} - 1\right],$$

$$f'(s) = \frac{2F(s)F'(s)\sin^2\theta_0}{(1 - F^2(s)\cos^2\theta_0)^2} = \frac{2F(s)F'(s)\sin^2\theta_0}{\sin^4\theta},$$

and so, if the value of s on the sheet is s_s,

$$ap(\boldsymbol{r}) = P^s \delta(\sin 2\phi - \sin 2\phi_s) = \frac{P^s \sin^4\theta \delta(s - s_s)}{2|F(s)F'(s)|\sin^2\theta_0} \tag{3.5}$$

and at the upstream limit $s_s = s_c$, $F(s) = 1$, $\theta = \theta_0$, and using

$$F'(s_c) = -\frac{(1 - B_c)}{s_c(1 - A_c)}$$

gives

$$ap(\boldsymbol{r}) = \frac{P^s \sin^2\theta_0 s_c(1 - A_c)}{2(1 - B_c)}\delta(s - s_c), \tag{3.6}$$

and since this must equal the pair density from the contact region, the upstream boundary condition on the sheet probability is

$$P^s(s_c, \theta_0, \pi/4) = \frac{2a(1 - A_c)}{3\Phi_c^3 \sin^2\theta_0}. \tag{3.7}$$

Returning to our general pair density function on the sheet, we integrate the Liouville equation (2.5) over a region $s_1 \leqslant s \leqslant s_2$, $\theta_1 \leqslant \theta_0 \leqslant \theta_2$, $\phi_1 \leqslant \phi \leqslant \phi_2$, where $\phi_1 \leqslant \phi_s(s, \theta_0) \leqslant \phi_2$ through the whole region. We apply the divergence theorem and note that the only sides which can contribute to the resulting surface integral are sides of constant s. The area element on these sides is

$$a^2 s^2 \sin\theta \, \mathrm{d}\theta \, \mathrm{d}\phi = a^2 s^2 F(s) \sin\theta_0 \, \mathrm{d}\theta_0 \, \mathrm{d}\phi,$$

and $\boldsymbol{e}_s$ is normal to the surfaces. Since s_1, s_2, θ_1 and θ_2 are arbitrary, this gives (after integrating over ϕ)

$$\frac{P^s \boldsymbol{V} \cdot \boldsymbol{e}_s}{2 \cos 2\phi_s} a^2 s^2 F(s) \sin\theta_0 = \mathscr{G}(\theta_0) \tag{3.8}$$

independent of s. From (2.7), we know that on the sheet,

$$\boldsymbol{V} \cdot \boldsymbol{e}_s = as\dot{\epsilon}(1 - A(s))(1 - F^2(s) \cos^2\theta_0) \cos 2\phi_s,$$

so this becomes

$$\tfrac{1}{2} P^s \dot{\epsilon}(1 - A(s))(1 - F^2(s) \cos^2\theta_0) a^3 s^3 F(s) \sin\theta_0 = \mathscr{G}(\theta_0),$$

and then the boundary condition (3.7) gives

$$\mathscr{G}(\theta_0) = \frac{a^4 s_c^3 \dot{\epsilon} \sin\theta_0}{3\Phi_c^3}.$$

The quantity required for later stress calculations is

$$\begin{aligned} \int_\phi p(\boldsymbol{r}) \, \mathrm{d}^3\boldsymbol{r} &= \int_\phi \frac{P^s \delta(\sin 2\phi - \sin 2\phi_s)}{a} a^3 s^2 \sin\theta \, \mathrm{d}\phi \, \mathrm{d}\theta \, \mathrm{d}s \\ &= \frac{P^s}{2a \cos 2\phi_s} a^3 s^2 \sin\theta \, \mathrm{d}\theta \, \mathrm{d}s = \frac{a^4 s_c^3 \dot{\epsilon} \sin\theta_0}{3\Phi_c^3 \boldsymbol{V} \cdot \boldsymbol{e}_s} \, \mathrm{d}\theta_0 \, \mathrm{d}s \\ &= \frac{a^3 \sin\theta_0 \, \mathrm{d}\theta_0}{3(1 - F^2(s) \cos^2\theta_0) \cos 2\phi_s} q(s) F^3(s) s^2 \, \mathrm{d}s. \end{aligned} \tag{3.9}$$

4. Contact force

Away from the contact region of the flow, the particles move unaffected by contact and the contact force F_c is zero. Within the contact region, the force was calculated in Wilson & Davis (2000), and for our form of $\boldsymbol{E}$ is

$$F_c = \frac{3\pi\mu a^2 s_c (1 - A_c) \boldsymbol{n} \cdot \boldsymbol{E} \cdot \boldsymbol{n}}{G_c} = \frac{3\pi\mu\dot{\epsilon} a^2 s_c (1 - A_c)}{G_c} \sin^2\theta \cos 2\phi, \tag{4.1}$$

where the mobility function $G(s)$ was introduced by Batchelor (1977).

5. Analytic stress results

Having calculated the pair distribution function in each of the regions above, and the contact force, it is straightforward to evaluate the three hydrodynamic integrals (from bulk, contact and sheet regions) and the direct contact integral contributing to the macroscopic rheology (2.4). In the case of the bulk and sheet regions, the contributions can be reduced to integrals over s only; in the case of the contact region, both the contributions can be found directly.

We will sum the contributions from the three regions, to express the results as

$$\mu^* = \mu\left[\tfrac{5}{2}c + kc^2 + O(c^3)\right]; \qquad k = \tfrac{5}{2} + k_{bulk} + k^H_{contact} + k^C_{contact} + k_{sheet}, \tag{5.1}$$

$$N_2 = c^2\mu\dot{\epsilon}\Psi_2 + O(c^3); \qquad \Psi_2 = \Psi_{bulk} + \Psi^H_{contact} + \Psi^C_{contact} + \Psi_{sheet}, \tag{5.2}$$

where

$$k_{bulk} = \frac{1}{4\pi}\int_{s=s_c}^{\infty}\left(\frac{1-F^2}{2}\right)^{1/2}\arcsin\left(\frac{2F^2}{1+F^2}\right)^{1/2}(60K + 5(7-F^2)L + (1-F^2)(7+3F^2)M)qs^2\,\mathrm{d}s + \frac{1}{4\pi}\int_{s=s_c}^{\infty}(1-F^2)(5L+(1-3F^2)M)Fqs^2\,\mathrm{d}s + \frac{15}{2}\int_{s=s_c}^{\infty}\left(1-\frac{2}{\pi}\arctan F\right)Jqs^2\,\mathrm{d}s, \tag{5.3a}$$

$$k^H_{contact} = \frac{5s_c^3 J_c}{4(1-B_c)\Phi_c^3}, \tag{5.3b}$$

$$k^C_{contact} = \frac{3s_c^5(1-A_c)^2}{80(1-B_c)G_c\Phi_c^3}, \tag{5.3c}$$

$$k_{sheet} = \frac{5}{4\pi}\int_{s=s_c}^{\infty}(L+M(1-F^2))F^3qs^2\,\mathrm{d}s + \frac{5}{2\pi}\int_{s=s_c}^{\infty}\left(\frac{1-F^2}{2}\right)^{3/2}\arcsin\left(\frac{2F^2}{1+F^2}\right)^{1/2} \times\left(\frac{4K}{(1-F^2)^2}+\frac{3L}{(1-F^2)}+M\right)F^2qs^2\,\mathrm{d}s. \tag{5.3d}$$

There is little to be gained by combining these terms so the total viscosity is not printed here. For the normal stress difference,

$$\Psi_{bulk} = \frac{1}{\pi}\int_{s=s_c}^{\infty}[(3F^2-5)M - 10L]F^3qs^2\,\mathrm{d}s, \tag{5.4a}$$

$$\Psi^H_{contact} = -\frac{2s_c^3(5L_c+M_c)}{3\pi(1-B_c)\Phi_c^3}, \tag{5.4b}$$

$$\Psi^C_{contact} = -\frac{3s_c^5(1-A_c)^2}{20\pi(1-B_c)G_c\Phi_c^3}, \tag{5.4c}$$

$$\Psi_{sheet} = \frac{5}{\pi}\int_{s=s_c}^{\infty}(2L+M(1-F^2))F^3qs^2\,\mathrm{d}s, \tag{5.4d}$$

and the combination simplifies to

$$\Psi_2 = -\frac{2}{\pi}\left[\int_{s_c}^{\infty}MF^5qs^2\,\mathrm{d}s + \frac{s_c^3}{(1-B_c)\Phi_c^3}\left(\frac{(5L_c+M_c)}{3}+\frac{3s_c^2(1-A_c)^2}{40G_c}\right)\right]. \tag{5.5}$$

We check the limit $s_c \to 2$, in which $\Phi_c \to \infty$ and $F(s) \to 0$, to have:

$$k \to \tfrac{5}{2} + \tfrac{15}{2}\int_2^{\infty}Jqs^2\,\mathrm{d}s, \quad \Psi_2 \to 0, \tag{5.6}$$

as required. We also note the specific asymptotic forms of the contact contributions for small ζ (using the near-field asymptotics given by, for example, Kim & Karrila

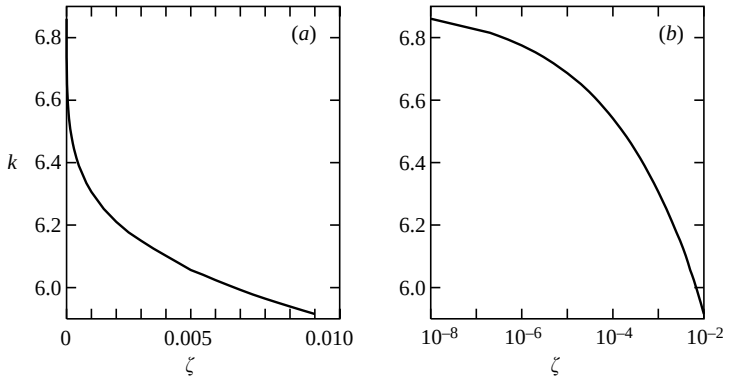

FIGURE 2. Plots of the c^2 viscosity coefficient k against the roughness height ζ. In (b), the ζ-axis is on a log scale to demonstrate that k behaves correctly as $\zeta \to 0$.

1991):

$$k^H_{contact} \sim 3.55\zeta^{0.22}(\log \zeta^{-1})^{-0.29}, \qquad k^C_{contact} \sim 5.095\zeta^{1.22}(\log \zeta^{-1})^{-0.29},$$
$$\Psi^H_{contact} \sim -5.49\zeta^{0.22}(\log \zeta^{-1})^{-0.29}, \qquad \Psi^C_{contact} \sim -6.486\zeta^{1.22}(\log \zeta^{-1})^{-0.29},$$

and observe that in the small-roughness limit, the direct contributions from the contact force are smaller than the hydrodynamic contact contributions by a factor of ζ.

6. Numerical results and discussion

6.1. *Numerical viscosity results*

An example set of viscosity results is shown in figure 2, with k plotted against ζ. As expected, the limit $\zeta \to 0$ is that of smooth spheres, for which $k = k^{smooth} \approx 6.9$. Batchelor & Green (1972*a*), Zinchenko (1984) and Kim & Mifflin (1985) reported $k^{smooth} = 7.6$, 7.0 and 7.1, respectively, with the small differences being due to the accuracies of the mobility functions employed. The latter two are thought to be the most accurate, and our result is 6.9, using a combination of the mobility data from Kim & Mifflin (1985) and far- and near-field asymptotics.

The viscosity is always lower for rough spheres than for smooth ones, with the effect being more marked for larger roughness heights. The physical explanation of this lowering in stress is that the closest approach of the particles is limited, limiting the magnitude of the lubrication stresses between the particles.

The values of the viscosity coefficient are very similar to those calculated for biaxial expansion flows (Wilson & Davis 2000) and for shear flows (Bergenholtz *et al.* 2002). In the latter case, reading from figure 11 of Bergenholtz *et al.* (2002) and converting to our notation gives four values for direct comparison (table 1). The trends in these two quantities are clearly the same; but we should not read too much into the specific numerical values since the shear values are calculated at finite (large) Péclet number and it is not clear from the graphs in Bergenholtz *et al.* (2002) that the zero-diffusion result has been reached.

6.2. *Numerical normal stress results*

The normal stress results are shown in figure 3, with $-\Psi_2$ plotted against ζ. As expected, the limit $\zeta \to 0$ is that of smooth spheres, for which $\Psi_2 = 0$. For all non-zero values of ζ, the normal stress is negative, and the values are significant for relatively small

ζ	k_{shear}	k_{strain}
2×10^{-5}	6.0	6.7
2×10^{-3}	5.9	6.2
2×10^{-2}	5.7	5.7
2×10^{-1}	5.7	4.9

TABLE 1. A direct comparison of values of the viscosity coefficient k for plane strain with that for shear flow from figure 11 of Bergenholtz *et al.* (2002).

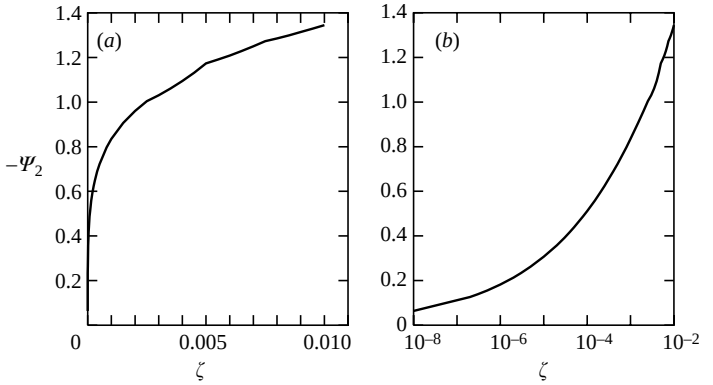

FIGURE 3. Plot of the negative c^2 coefficient of normal stress, Ψ_2, against the roughness height ζ. In (*b*), the ζ-axis is on a log scale to demonstrate that $\Psi_2 \to 0$ as $\zeta \to 0$.

roughness heights: for a roughness height of $\zeta = 10^{-3}$, within the ranges predicted by Smart & Leighton (1989) and Ekiel-Jeżewska *et al.* (1999), we have $\Psi_2 = -0.83$ and $N_2 = -0.83c^2\mu\dot{\epsilon}$.

6.3. *The effect of Brownian motion*

In order to add a small amount of Brownian motion to our system, two modifications must be made. First, the equation governing the pair distribution function (2.5) becomes

$$\nabla\cdot[p(\boldsymbol{r})\boldsymbol{V}(\boldsymbol{r})] - Pe^{-1}\nabla\cdot[\boldsymbol{D}(\boldsymbol{r})\cdot\nabla p(\boldsymbol{r})] = 0 \tag{6.1}$$

in which lengths are made dimensionless with a, velocities with $a\dot{\epsilon}$, and the diffusivity tensor with $kT/6\pi\mu a$. The (large) Péclet number is defined as $Pe = 6\pi\mu a^3\dot{\epsilon}/kT$ and the dimensionless diffusivity tensor is $D_{ij} = G(s)n_in_j + H(s)(\delta_{ij} - n_in_j)$ as in Batchelor (1977). The contact boundary condition on this equation becomes a zero-flux condition at $r = as_c$:

$$p\boldsymbol{V}\cdot\boldsymbol{n} - Pe^{-1}[\boldsymbol{D}\cdot\nabla p]\cdot\boldsymbol{n} = 0, \tag{6.2}$$

while in the far-field we retain the boundary condition that $p(\boldsymbol{r}) \to 1$ as $r \to \infty$, as for the non-Brownian case. Second, an extra Brownian stress contribution is added to (2.4). This extra stress is always $O(Pe^{-1})$, so we continue to neglect it; but the changes to the pair distribution function may be important even for large Pe.

Brady & Morris (1997) considered this system, with hard-sphere repulsion, in various flow types, and found a boundary layer of $O(Pe^{-1})$ in the compressive region. Because they were considering many different linear flows, they neglected angular

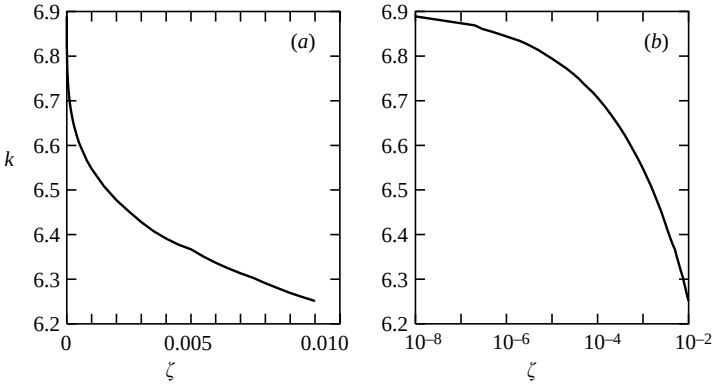

FIGURE 4. Plots of the c^2 viscosity coefficient k against the roughness height ζ, neglecting the effect of the sheet and wake regions.

terms in (6.1) when solving for the value of p within the boundary layer. They commented on this approximation (Brady & Morris 1997, p. 118): 'The $O(Pe^{-1})$ terms neglected, including the velocity divergence term, affect the precise value of p, but do not affect the scaling with Pe'; while this is true for any specific finite value of ζ, for very small roughness heights the size of the neglected terms may be large, and in all cases they are at least as large as some of the terms which are retained.

For the specific case of plane strain flow, and using the insight provided by the calculations of § 3, we can solve (6.1) self-consistently (i.e. without using the radial balance approximation) to leading order in Pe^{-1}, obtaining the solution close to contact:

$$p \sim -Pe\frac{s_c^2(1-A_c)\sin^2\theta\cos 2\phi}{3G_c(1-B_c)\Phi_c^3}\exp\left[\frac{Pe\,s_c(1-A_c)\sin^2\theta\cos 2\phi}{G_c}(s-s_c)\right]. \tag{6.3}$$

Full details of this calculation are given in Appendix A.

There are several points to note about this solution. First, the dimensionless width of the boundary layer is proportional to $G_c/[Pe\,s_c(1-A_c)\sin^2\theta\cos 2\phi]$ which is of order Pe^{-1}, as indicated by Brady & Morris (1997). Secondly, in the limit of large Pe, if we integrate over a region which is large relative to the boundary layer, but small compared to all other distances, we obtain

$$\int_{r=as_c}^{as_c+\epsilon} p\,\mathrm{d}r \sim \frac{as_c}{3(1-B_c)\Phi_c^3}, \tag{6.4}$$

which corresponds with the result from integrating our contact pair density P^c of § 3.3.

Finally, we note that the width of the boundary layer is inversely proportional to

$$\boldsymbol{n}\cdot\boldsymbol{E}\cdot\boldsymbol{n} = \dot{\epsilon}\sin^2\theta\cos 2\phi$$

where this is negative; so at the end of the compressive quadrant where $\boldsymbol{n}\cdot\boldsymbol{E}\cdot\boldsymbol{n}=0$, the boundary-layer structure breaks down. It is only valid where $|\boldsymbol{n}\cdot\boldsymbol{E}\cdot\boldsymbol{n}| > Pe^{-1}$. We can therefore expect that even a small amount of Brownian motion will have a large effect on the sheet-and-wake structure we have predicted in the non-Brownian case. We cannot predict quantitatively the form of $p(\boldsymbol{r})$ in the extensional quadrants of the flow, but in figures 4 and 5 we plot the values of k and $-\Psi_2$ which would be predicted if the pair density in the extensional region were simply $q(s)$: that is, the stresses affected only by the compressive region (this approximation is liable to be

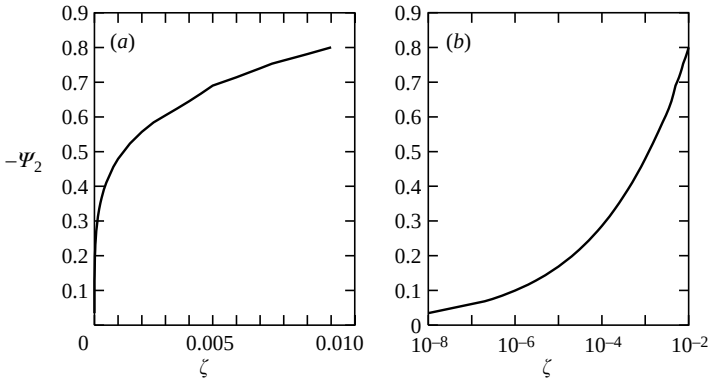

FIGURE 5. Plots of the negative c^2 coefficient of normal stress, $-\Psi_2$, against roughness height ζ, neglecting the effect of the sheet and wake regions.

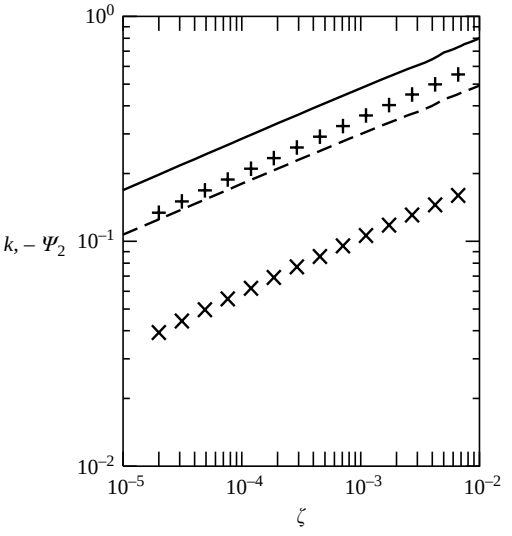

FIGURE 6. Plot of compressive region contributions to the c^2 stress coefficients. The curves are from the calculation in this paper: $-\Psi_2$ (solid line), and k (dotted line). The points are taken from Brady & Morris (1997, figure 4): $-\Psi_2$ (+) and k (×).

an over-prediction of the effect of diffusion). These figures are exactly equivalent to figures 2 and 3 for the non-Brownian case. In particular, we note the reduction in magnitude of the normal stress difference: at $\zeta = 10^{-3}$ where we had $\Psi_2 = -0.83$ with the sheet and wake included, we now have $\Psi_2 = -0.48$.

Brady & Morris (1997) studied this system for all Péclet numbers, and found that a high-*Pe* asymptote was reached for $Pe \sim 10^4$. This being so, in their figure 4, they took a Péclet number of 10^6 and plotted compressive region stresses against hard-sphere separation height, plotting two quantities which in our notation are

$$-I_2 = -\frac{2\pi}{15}\left(\Psi^H_{contact} + \Psi^C_{contact}\right), \quad I_\eta = \frac{4\pi}{15}\left(k^H_{contact} + k^C_{contact}\right),$$

against a contact height parameter $b/a - 1 = \zeta/2$. In figure 6, we show our equivalent terms: that is, the same values of Ψ_2 as in figure 5, and the values of k minus the

contribution from the reduced bulk region $s > s_c$. The results from Brady & Morris (1997) are also plotted on the same graph for comparison. It is noted that, because their angular form of the contact pair distribution is not quantitatively correct, we do not have quantitative agreement (our results have slightly larger magnitude in both cases); but the power-law trend for small ζ is in agreement between our results and theirs.

7. Concluding remarks

We have investigated analytically the rheology to $O(c^2)$ of a dilute suspension of rough spheres in a planar straining flow. For perfectly smooth particles, the stress is Newtonian and can be represented by a scalar viscosity which is approximately $1 + 5c/2 + 6.9c^2$ times the solvent viscosity for a concentration c of particles. In contrast, when particles are allowed to come into contact through a microscopic surface roughness, a negative second normal stress difference is caused. In addition, the hard-sphere repulsion lowers the viscosity (which is an effect already discussed for axisymmetric strain in three dimensions (Wilson & Davis 2000) and shear in two dimensions (Wilson & Davis 2002)). We give quantitative results both for the artificial case of no Brownian motion, and the asymptotic limit of small Brownian motion. These are in qualitative agreement with Brady & Morris (1997), but within the boundary layer which they identified, we are able to calculate fully the angular dependence of the pair distribution function, which they calculated only approximately.

The author would like to thank Robert H. Davis and John M. Rallison for helpful discussions, Jeffrey F. Morris for providing the data from Brady & Morris (1997), and the referees for their many helpful suggestions. This work was supported in part by the Nuffield Foundation NUF-NAL/00620/G (2002).

Appendix. Boundary-layer structure for a system with large Pe

Here we start from the dimensionless governing equation (6.1):

$$\nabla \cdot [p(\boldsymbol{r})\boldsymbol{V}(\boldsymbol{r})] - Pe^{-1}\nabla \cdot [\boldsymbol{D}(\boldsymbol{r}) \cdot \nabla p(\boldsymbol{r})] = 0 \tag{A 1}$$

with boundary conditions

$$p\boldsymbol{V} \cdot \boldsymbol{n} - Pe^{-1}[\boldsymbol{D} \cdot \nabla p] \cdot \boldsymbol{n} = 0 \ \text{ at } s = s_c, \tag{A 2}$$

$$p \to 1 \ \text{ as } s \to \infty. \tag{A 3}$$

We define three quantities, γ_i, the dimensionless components of $\boldsymbol{E} \cdot \boldsymbol{n}$, which are related to the free velocity:

$$\gamma_r = \sin^2\theta \cos 2\phi, \tag{A 4a}$$

$$\gamma_\theta = \sin\theta \cos\theta \cos 2\phi, \tag{A 4b}$$

$$\gamma_\phi = -\sin\theta \sin 2\phi, \tag{A 4c}$$

$$V_r = s(1 - A)\gamma_r, \tag{A 5a}$$

$$V_\theta = s(1 - B)\gamma_\theta, \tag{A 5b}$$

$$V_\phi = s(1 - B)\gamma_\phi, \tag{A 5c}$$

to rewrite (A 1) in spherical polars as

$$\frac{1}{s^2}\frac{\partial}{\partial s}(ps^3(1-A)\gamma_r)+\frac{1}{s\sin\theta}\frac{\partial}{\partial\theta}(\sin\theta ps(1-B)\gamma_\theta)+\frac{1}{s\sin\theta}\frac{\partial}{\partial\phi}(ps(1-B)\gamma_\phi)$$
$$-Pe^{-1}\frac{1}{s^2}\frac{\partial}{\partial s}\left(Gs^2\frac{\partial p}{\partial s}\right)-Pe^{-1}\frac{H}{s^2\sin\theta}\frac{\partial}{\partial\theta}\left(\sin\theta\frac{\partial p}{\partial\theta}\right)-Pe^{-1}\frac{H}{s^2\sin^2\theta}\frac{\partial^2 p}{\partial\phi^2}=0, \quad (A\,6)$$

which may also be expanded:

$$s(1-A)\gamma_r\frac{\partial p}{\partial s}+(1-B)\left[\gamma_\theta\frac{\partial p}{\partial\theta}+\frac{\gamma_\phi}{\sin\theta}\frac{\partial p}{\partial\phi}\right]$$
$$+\left[\gamma_r(3(1-A)-sA')+\frac{1-B}{\sin\theta}\left(\frac{\partial}{\partial\theta}(\sin\theta\gamma_\theta)+\frac{\partial\gamma_\phi}{\partial\phi}\right)\right]p$$
$$-\frac{Pe^{-1}}{s^2}\left[Gs^2\frac{\partial^2 p}{\partial s^2}+(2sG+s^2G')\frac{\partial p}{\partial s}+H\frac{\partial^2 p}{\partial\theta^2}+\frac{H\cos\theta}{\sin\theta}\frac{\partial p}{\partial\theta}+\frac{H}{\sin^2\theta}\frac{\partial^2 p}{\partial\phi^2}\right]=0, \quad (A\,7)$$

in which we have used A' to denote $\mathrm{d}A/\mathrm{d}s$; and (A 2) becomes

$$s\gamma_r(1-A)p-GPe^{-1}\frac{\partial p}{\partial s}=0 \text{ at } s=s_c. \quad (A\,8)$$

A.1. *Outer solution*

Where there are no large gradients in p, we can neglect the Pe^{-1} terms of (A 6) to obtain

$$\frac{1}{s^2}\frac{\partial}{\partial s}(s^3(1-A)\gamma_r p)+\frac{1}{s\sin\theta}\frac{\partial}{\partial\theta}(\sin\theta s(1-B)\gamma_\theta p)+\frac{1}{s\sin\theta}\frac{\partial s(1-B)\gamma_\phi p}{\partial\phi}=0 \quad (A\,9)$$

which can be solved using $p=q(s)$ where

$$q(s)=\frac{1}{(1-A)}\exp\int_s^\infty\frac{3(B-A)}{s'(1-A)}\,\mathrm{d}s', \quad (A\,10)$$

satisfying the outer but not the inner boundary condition.

A.2. *Inner boundary-layer solution*

In the compressive region where $\gamma_r<0$, we assume that there is a boundary-layer of width δ close to the contact surface. We introduce a strained coordinate $z=(s-s_c)/\delta$ and (A 7) becomes

$$\delta^{-1}s(1-A)\gamma_r\frac{\partial p}{\partial z}+(1-B)\left[\gamma_\theta\frac{\partial p}{\partial\theta}+\frac{\gamma_\phi}{\sin\theta}\frac{\partial p}{\partial\phi}\right]+\left[\gamma_r(3(1-A)-sA')\right.$$
$$\left.+\frac{1-B}{\sin\theta}\left(\frac{\partial}{\partial\theta}(\sin\theta\gamma_\theta)+\frac{\partial\gamma_\phi}{\partial\phi}\right)\right]p-\frac{Pe^{-1}}{s^2}\left[\delta^{-2}Gs^2\frac{\partial^2 p}{\partial z^2}+\delta^{-1}(2sG+s^2G')\frac{\partial p}{\partial z}\right.$$
$$\left.+H\frac{\partial^2 p}{\partial\theta^2}+\frac{H\cos\theta}{\sin\theta}\frac{\partial p}{\partial\theta}+\frac{H}{\sin^2\theta}\frac{\partial^2 p}{\partial\phi^2}\right]=0, \quad (A\,11)$$

in which the first term is comparable to the term $(Pe^{-1}/s^2)[\delta^{-2}Gs^2\partial^2 p/\partial z^2]$ from the middle line if $\delta^{-1}=\alpha Pe$. Selecting this scaling and neglecting terms of order Pe^{-1}, we obtain

$$\alpha Pe\left[s(1-A)\gamma_r\frac{\partial p}{\partial z}-\alpha G\frac{\partial^2 p}{\partial z^2}\right]-\alpha\left(\frac{2G}{s}+G'\right)\frac{\partial p}{\partial z}+(1-B)\left[\gamma_\theta\frac{\partial p}{\partial\theta}+\frac{\gamma_\phi}{\sin\theta}\frac{\partial p}{\partial\phi}\right]$$
$$+\gamma_r(3(1-A)-sA')p+\left[\frac{1-B}{\sin\theta}\left(\frac{\partial}{\partial\theta}(\sin\theta\gamma_\theta)+\frac{\partial\gamma_\phi}{\partial\phi}\right)\right]p=0 \quad (A\,12)$$

with inner boundary condition

$$s_c\gamma_r(1-A_c)p - G_c\alpha\frac{\partial p}{\partial z} = 0 \quad \text{at } z=0, \tag{A 13}$$

and an outer condition that the solution must match onto the outer solution for large z. For convenience, we will choose

$$\alpha = \frac{s_c(1-A_c)}{G_c}. \tag{A 14}$$

We pose an asymptotic series

$$p = p_0 + Pe^{-1}p_1 + \cdots$$

and expand mobility functions as $A = A_c + \delta z A_c' + \cdots$ to obtain, at leading order,

$$\gamma_r\frac{\partial p_0}{\partial z} - \frac{\partial^2 p_0}{\partial z^2} = 0, \tag{A 15}$$

with solution

$$\begin{aligned} p_0 &= f_0(\theta,\phi)\exp[\gamma_r z] + g_0(\theta,\phi) \\ &= f_0(\theta,\phi)\exp\left[\frac{s_c(1-A_c)\gamma_r Pe(s-s_c)}{G_c}\right] + g_0(\theta,\phi). \end{aligned} \tag{A 16}$$

We cannot satisfy the outer boundary condition with this function; we can satisfy the inner condition, and doing so gives $g_0 = 0$.

We return to (A 12) and obtain, at order 1, the PDE:

$$\begin{aligned} &\frac{s_c(1-A_c)}{G_c}\left[s_c(1-A_c)\gamma_r\frac{\partial p_1}{\partial z} - s_c(1-A_c)\frac{\partial^2 p_1}{\partial z^2}\right] \\ &= -z\left[(1-A_c-s_cA_c')\gamma_r\frac{\partial p_0}{\partial z} - \frac{s_c(1-A_c)}{G_c}G_c'\frac{\partial^2 p_0}{\partial z^2}\right] \\ &\quad + \frac{s_c(1-A_c)}{G_c}\left(\frac{2G_c}{s_c}+G_c'\right)\frac{\partial p_0}{\partial z} - (1-B_c)\left[\gamma_\theta\frac{\partial p_0}{\partial\theta} + \frac{\gamma_\phi}{\sin\theta}\frac{\partial p_0}{\partial\phi}\right] \\ &\quad - \left[\gamma_r(3(1-A_c)-s_cA_c') + \frac{1-B_c}{\sin\theta}\left(\frac{\partial}{\partial\theta}(\sin\theta\gamma_\theta) + \frac{\partial\gamma_\phi}{\partial\phi}\right)\right]p_0, \end{aligned} \tag{A 17}$$

which we may write as

$$\frac{s_c^2(1-A_c)^2}{G_c}\left[\gamma_r\frac{\partial p_1}{\partial z} - \frac{\partial^2 p_1}{\partial z^2}\right] = (\beta_1 z f_0 - \beta_2 + \beta_3 f_0)\exp[\gamma_r z] \tag{A 18}$$

with parameters which depend only on θ and ϕ:

$$\beta_1 = \beta_4\gamma_r^2 - (1-B_c)\left[\gamma_\theta\frac{\partial\gamma_r}{\partial\theta} + \frac{\gamma_\phi}{\sin\theta}\frac{\partial\gamma_r}{\partial\phi}\right], \tag{A 19a}$$

$$\beta_2 = (1-B_c)\left[\gamma_\theta\frac{\partial f_0}{\partial\theta} + \frac{\gamma_\phi}{\sin\theta}\frac{\partial f_0}{\partial\phi}\right], \tag{A 19b}$$

$$\beta_3 = \beta_4\gamma_r - (1-B_c)\left(\frac{\cos\theta}{\sin\theta}\gamma_\theta + \frac{\partial\gamma_\theta}{\partial\theta} + \frac{1}{\sin\theta}\frac{\partial\gamma_\phi}{\partial\phi}\right), \tag{A 19c}$$

$$\beta_4 = s_cA_c' + A_c - 1 + \frac{G_c's_c(1-A_c)}{G_c}. \tag{A 19d}$$

Solving for p_1 gives

$$p_1 = -\frac{G_c}{s_c^2(1-A_c)^2\gamma_r}\left(\frac{\beta_1 f_0 z^2}{2} - \left(\frac{\beta_1 f_0}{\gamma_r} + \beta_2 - \beta_3 f_0\right)\left[z - \frac{1}{\gamma_r}\right]\right)\exp[\gamma_r z] + f_1(\theta,\phi)\exp[\gamma_r z] + g_1(\theta,\phi) \tag{A 20}$$

and applying the inner boundary condition gives

$$g_1(\theta,\phi) = \frac{G_c}{s_c^2(1-A_c)^2\gamma_r^2}\left(\frac{\beta_1 f_0}{\gamma_r} + \beta_2 - \beta_3 f_0\right). \tag{A 21}$$

Finally, we apply the matching condition for large z, that

$$p_0 + Pe^{-1}p_1 \sim q_c \text{ as } z \to \infty, \tag{A 22}$$

which gives

$$g_1(\theta,\phi) = Peq_c. \tag{A 23}$$

Using (A 21) and substituting the definitions (A 19) of the angular parameters β_i, and (A 4) of the parameters γ_i, this becomes a PDE for $f_0(\theta,\phi)$:

$$\sin\theta\cos\theta\cos^2 2\phi\frac{\partial f_0}{\partial\theta} - \sin 2\phi\cos 2\phi\frac{\partial f_0}{\partial\phi} - (\sin^2\theta\cos^2 2\phi + 2)f_0 = Peq_c\frac{s_c^2(1-A_c)^2\sin^4\theta\cos^3 2\phi}{G_c(1-B_c)}. \tag{A 24}$$

This equation is solved by

$$f_0(\theta,\phi) = -Pe\,q_c\frac{s_c^2(1-A_c)^2}{3G_c(1-B_c)}\sin^2\theta\cos 2\phi, \tag{A 25}$$

giving the leading-order boundary-layer solution as

$$p = -Pe\,q_c\frac{s_c^2(1-A_c)^2}{3G_c(1-B_c)}\sin^2\theta\cos 2\phi\exp\left[\frac{Pe\,s_c(1-A_c)(s-s_c)\sin^2\theta\cos 2\phi}{G_c}\right] \tag{A 26}$$

as in (6.3).

A.3. *Scaling breakdown*

The size of the boundary-layer is of order $[Pe\sin^2\theta\cos 2\phi]^{-1}$, which suggests that close to $\phi = \pi/4$ where $\cos 2\phi$ (and hence γ_r) becomes small, our scaling will break down and other terms will come into the leading-order balance.

This occurs, in fact, when $\gamma_r \sim Pe^{-1/3}$, when our two dominant terms are of order $Pe^{1/3}$ and are balanced by the angular advection term

$$\frac{1}{s\sin\theta}\frac{\partial}{\partial\phi}(ps(1-B)\gamma_\phi). \tag{A 27}$$

In this region, if we introduce two strained coordinates, $y = Pe^{2/3}(s-s_c)$ and $\psi = Pe^{1/3}(\phi - \pi/4)$, then the leading-order PDE (from (A 7)) becomes

$$-G_c\frac{\partial^2 p}{\partial y^2} - 2s_c(1-A_c)\sin^2\theta\psi\frac{\partial p}{\partial y} - (1-B_c)\frac{\partial p}{\partial\psi} = 0, \tag{A 28}$$

for which a solution satisfying the boundary conditions has not yet been found.

A.4. *Sheet and wake in the extensional region*

Assuming that the boundary layer is advected to the separation point $\phi = \pi/4$, within the extensional quadrant of the flow this high-concentration region (the sheet) will diffuse as s increases, since there is now no advective flux in the correct direction to maintain steep gradients in p. The width of the diffuse sheet region scales as $(Pe^{-1}s)^{1/2}$, as we expect for a diffusion equation, and so the largest extent (in s) over which it may still be expected to contribute to the rheology scales as Pe.

It may, however, be possible that the effective extent of the sheet and wake together is much less: the wake region has a dimension in the y-direction of order s^{-1}, and the contribution could be negligible once the sheet has diffused to the edge of the wake. This happens over a shorter lengthscale of order $Pe^{1/3}$.

REFERENCES

Batchelor, G. K. 1967 *An Introduction to Fluid Dynamics*. Cambridge University Press.

Batchelor, G. K. 1977 The effect of Brownian motion on the bulk stress in a suspension of spherical particles. *J. Fluid Mech.* **83**, 97–117.

Batchelor, G. K. & Green, J. T. 1972*a* The determination of the bulk stress in a suspension of spherical particles to order c^2. *J. Fluid Mech.* **56**, 401–427.

Batchelor, G. K. & Green, J. T. 1972*b* The hydrodynamic interaction of two small freely-moving spheres in a linear flow field. *J. Fluid Mech.* **56**, 375–400.

Bergenholtz, J., Brady, J. F. & Vicic, M. 2002 The non-Newtonian rheology of dilute colloidal suspensions. *J. Fluid Mech.* **456**, 239–275.

Brady, J. F. 1993 Brownian motion, hydrodynamics, and the osmotic pressure. *J. Chem. Phys.* **98**, 3335–3341.

Brady, J. F. & Morris, J. F. 1997 Microstructure of strongly sheared suspensions and its impact on rheology and diffusion. *J. Fluid Mech.* **348**, 103–139.

Davis, R. H. 1992 Effects of surface roughness on a sphere sedimenting through a dilute suspension of neutrally buoyant spheres. *Phys. Fluids* **4**, 2607–2619.

Einstein, A. 1906 Eine neue Bestimmung der Moleküledimensionen. *Annln Phys.* **19**, 289–306.

Einstein, A. 1911 Berichtigung zu meiner Arbeit: 'Eine neue Bestimmung der Moleküledimensionen'. *Annln Phys.* **34**, 591–592.

Ekiel-Jeżewska, M. L., Feuillebois, F., Lecoq, N., Masmoudi, K., Anthore, R., Bostel, F. & Wajnryb, E. 1999 Hydrodynamic interactions between two spheres at contact. *Phys. Rev.* E **59**, 3182–3191.

Jeffrey, D. J., Morris, J. F. & Brady, J. F. 1993 The pressure moments for two rigid spheres in low-Reynolds-number flow. *Phys. Fluids* **5**, 2317–2325.

Kim, S. & Karrila, S. J. 1991 *Microhydrodynamics: Principles and Selected Applications*. Butterworth-Heinemann.

Kim, S. & Mifflin, R. T. 1985 The resistance and mobility functions of two equal spheres in low-Reynolds-number flow. *Phys. Fluids* **28**, 2033–2045.

Russel, W. B. 1980 Review of the role of colloidal forces in the rheology of suspensions. *J. Rheol.* **24**, 209–232.

Smart, J. R. & Leighton, D. T. 1989 Measurement of the hydrodynamic surface roughness of non-colloidal spheres. *Phys. Fluids* A **1**, 52–60.

Wilson, H. J. & Davis, R. H. 2000 The viscosity of a dilute suspension of rough spheres. *J. Fluid Mech.* **421**, 339–367.

Wilson, H. J. & Davis, R. H. 2002 Shear stress of a monolayer of rough spheres. *J. Fluid Mech.* **452**, 425–441.

Zinchenko, A. Z. 1984 Effect of hydrodynamic interactions between the particles on the rheological properties of dilute emulsions. *Prikl. Mat. Mekh.* **48**, 198–206.